

# Nucleotide Interaction with Chitosan Layer Deposited on Fumed Silica Surface: Practice and Theory towards Establishing the Mechanism at the Molecular Level

Tetyana M. Budnyak,<sup>1,2\*</sup> Nataliya N. Vlasova,<sup>2</sup> Lyudmila P. Golovkova,<sup>2</sup> Olga Markitan,<sup>2</sup>  
Glib Baryshnikov,<sup>3,4</sup> Hans Ågren,<sup>3,5</sup> Adam Slabon<sup>1</sup>

<sup>1</sup>Department of Materials and Environmental Chemistry, Stockholm University, Svante Arrhenius väg 16 C, 106 91 Stockholm, Sweden

<sup>2</sup>Chuiko Institute of Surface Chemistry of National Academy of Sciences of Ukraine, 17 General Naumov Str., 03164 Kyiv, Ukraine

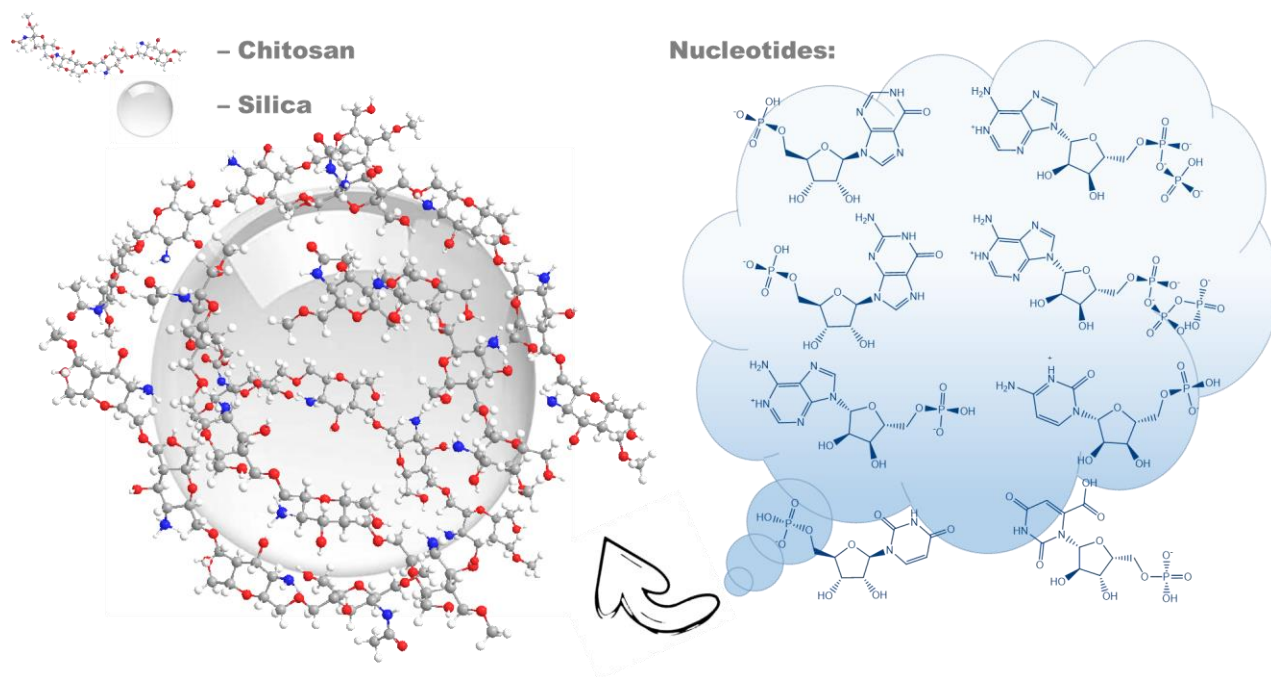
<sup>3</sup>Department of Physics and Astronomy, Uppsala University, Box 516, SE-751 20 Uppsala, Sweden

<sup>4</sup>Department of Chemistry and Nanomaterials Science, Bohdan Khmelnytsky National University, 18031, Cherkasy, Ukraine

<sup>5</sup>College of Chemistry and Chemical Engineering, Henan University, Kaifeng, Henan 475004, P. R. China

\*Corresponding author: Tetyana M. Budnyak, Svante Arrhenius väg 16 C, 106 91 Stockholm, Sweden, [tetyana.budnyak@mmk.su.se](mailto:tetyana.budnyak@mmk.su.se)

## Graphical abstract



## Abstract

The growing interest in gene therapy is coupled to the strong need for the development of safe and efficient gene transfection vectors. A composite based on chitosan and fumed silica has been found to be a prospective gene delivery carrier. This study presents an investigation of the nature of the bonds between a series of mono-, di- and triphosphate nucleotides with a chitosan layer deposited on a fumed silica surface. It was observed that the adsorption of most of the studied nucleotides is determined by the formation of one surface complex. Experimentally measured surface complex formation constants ( $\log K$ ) of the nucleotides were found to be in range 2.69–4.02 which is higher than that for the orthophosphate (2.39). Theoretically calculated nucleotide complexation energies for chitosan deposited on the surface range from 11.5 to 23.0 kcal·mol<sup>-1</sup> in agreement with experimental data. The adsorption of nucleotides was interpreted using their calculated speciation in aqueous solution. Based on the structures of all optimized complexes determined from quantum-chemical PM6 calculations, electrostatic interactions between the surface-located NH<sub>3</sub><sup>+</sup> groups and –PO<sub>3</sub>H<sup>-</sup>/–PO<sub>3</sub><sup>2-</sup> fragments of the nucleotides was identified to play the decisive role in the adsorption mechanism. The saccharide fragment of monophosphates also plays an important role in the binding of the nucleotides to chitosan through the creation of hydrogen bonds; in the case of di- and triphosphates the role of the saccharide fragment decreases significantly.

**Keywords:** nucleotides, chitosan, silica, adsorption, complexation, surface

## 1. Introduction

Gene therapy has proved to be an effective solution for most known diseases. The increased interest in gene therapy has called for proper materials to serve as safe and efficient gene transfection vectors [1]. Among biopolymers, chitosan and its derivatives represent perspective materials for a large number of applications, especially in the pharmaceutical, environmental and industrial fields [2–6]. These biopolymers, originating from marine waste, have attracted much attention as non-viral vectors due to their valuable properties as well as high positive charge density in low pH solution localized on the primary amino groups. Deoxyribonucleic acid (DNA) plasmids are non-viral vectors that can be delivered to the target cells as naked DNA or in association with different compounds such as liposomes, gelatin or polyamine nanospheres [7]. Their positively charged character enables chitosan to bind with the negatively charged DNA and ribonucleic acid (RNA) [8]. These beneficial features give chitosan the capability as gene carriers [9,10]. Some studies have reported the modification of chitosan for the purpose of improving the transfection

efficiency of chitosan formulations [11,12]. However, the interaction mechanism between chitosan and DNA is still unclear at the molecular level.

It has been proved that the activity of chitosan could even be increased when it is part of organic-inorganic composites [13,14]. Chitosan-silica composites deserve here special attention due to the complementary properties of silica towards polymers, e.g. resistance to the influence of microorganisms and high specific surface area [15–20].

Defining the interaction of a chitosan-silica composite with a biological medium is an extremely complex task. This is due to the formation of many different-in-nature bonds, involving numerous groups of biomolecules and surface functional groups of the chitosan and silica. The interaction of the composite surfaces with monomeric biomolecules – nucleotides, which are the structural units of nucleic acids, can serve as a subject for model studies. The aim of this work is to study the adsorption of nucleotides from aqueous solution onto chitosan-silica surfaces and to quantitatively estimate experimental data in terms of surface complexation theory. The study is supported by quantum-chemical calculations that provide understanding of the impact and the nature of bonds between the nucleotides (heterocyclic base, saccharide and phosphate groups) and chitosan.

## **2. Experimental part**

### *2.1. Materials*

Chitosan, Sigma Aldrich, No 417963, molecular weight from 190 to 370 kDa, degree of deacetylation not less than 75% and solubility 10 g·L<sup>-1</sup>; fumed silica, specific surface area 150 m<sup>2</sup>·g<sup>-1</sup>, obtained from State Enterprise “Kalush Test Experimental Plant of Institute of Surface Chemistry of National Academy of Sciences of Ukraine” were used for the synthesis. Nucleotides as sodium salts – adenosine-5'-monophosphate (Reanal), adenosine-5'-diphosphate (Alfa Aesar), adenosine-5'-triphosphate (Alfa Aesar), guanosine-5'-monophosphate (Reanal), inosine-5'-monophosphate (Sigma Aldrich), cytidine-5'-monophosphate (Reanal), uridine-5'-monophosphate (Reanal), orotidine-5'-monophosphate (Sigma Aldrich); sodium dihydrophosphate (Merck), and sodium chloride (Merck) were used without additional purification. The standard solution of HCl and NaOH (Titrisol, Merck) were used for pH adjusting.

### *2.2. Synthesis of chitosan-fumed silica composite.*

Chitosan-silica composite was synthesized under technic reported in our previous study [21]. Briefly, 10 g of fumed silica (A150) was impregnated by 100 ml of 1% chitosan solution in 2% acetic acid and stirred for a day. The obtained sample was dried at 50 °C overnight.

### *2.3 Potentiometric titration*

Potentiometric titration of the chitosan-silica composite suspension (1 g·L<sup>-1</sup>) with acid and base were performed at 20 °C (±1 °C) in gas-tight 50 mL centrifuge tubes (Falcon) in a thermostated water bath shaker. To each centrifuge tubes 0.02 g of composite, and 20 ml of 0.01 M NaCl solution were placed, then some amounts of HCl or NaOH solutions were added. After 24, 48, and 72 h of shaking the pH values were measured using an Inolab Level 2P pH meter (WTW) equipped with a combination electrode (SenTix81) and temperature probe. The electrode was calibrated using a 3-point calibration with commercial pH buffers (CertiPur, Merck) to a precision of pH 0.02 units. It was found that acid-base equilibrium achieved in 48 h. Electrode readings were taken when a drift less than 0.002 pH units in 10 min was attained.

#### 2.4 Sorption experiments

Nucleotide adsorption was studied at 20 °C (±1 °C). To each centrifuge tubes 0.02 g of composite, and 20 ml of 0.1 mmol·L<sup>-1</sup> nucleotide solution (in 0.01 M NaCl) were placed. The pH was adjusted to the desired value between 2 and 9 with HCl or NaOH solutions. All suspensions were stirred for 2 days, the final pH was measured, and then the solid phase was separated by centrifugation (8000 rpm, 10 min). It was preliminarily found that 2 days was sufficient time to reach adsorption equilibrium. Nucleotide concentrations were determined from the UV absorption spectra (Specord M-40 spectrophotometer, Carl Zeiss Jena). All components were characterized by the absorption bands near 260 nm. The pH dependences of the positions and intensities of the bands were determined beforehand. Orthophosphate concentrations in the solutions were determined as phosphoric molybdenum blue using Phosphate Test reagent kit (Spectroquant, Merck).

The amounts of adsorbed nucleotides and phosphate (as % of adsorption) were calculated as the difference between initial and equilibrium concentrations. Experimental adsorption values are shown in the figures as symbols, and the calculated adsorption curves are shown as lines.

Langmuir, Freundlich and Temkin isotherm models were applied to analyze the adsorption of ATP by chitosan deposited on silica surface. The linear form of the Langmuir model [22]:

$$\frac{c_e}{q_e} = \frac{c_e}{q_o} + \frac{1}{K_L q_o},$$

where  $c_e$  is the equilibrium concentration of molecules (mmol/L),  $q_e$  is the amount of the adsorbed molecules (mmol·g<sup>-1</sup>), and  $q_o$  and  $K_L$  are the Langmuir constants related to the adsorption capacity (mmol·g<sup>-1</sup>) and the equilibrium constant (L·mg<sup>-1</sup>), respectively.

The Freundlich model [23]:

$$\log q_e = \log K_F + \frac{1}{n} \cdot \log c_e,$$

where:  $K_F$  and  $n$  are the Freundlich constants related to the sorption capacity and the sorption intensity, respectively.

The Temkin model:

$$c_s = \frac{RT}{b_T} \ln(K_T) + \frac{RT}{b_T} \ln c_{eq}$$

where  $c_s$  is the concentration of molecule in the solid phase ( $\text{mol}\cdot\text{g}^{-1}$ ),  $K_T$  is the model constant ( $\text{L}\cdot\text{g}^{-1}$ ),  $R$  is the gas constant ( $8.314 \text{ J}\cdot\text{mol}^{-1}\cdot\text{K}^{-1}$ ),  $T$  represents the absolute temperature (K), and  $c_{eq}$  denotes the equilibrium concentration of molecules ( $\text{mol}\cdot\text{L}^{-1}$ ) in the aqueous phase.

## 2.5. Model Calculations

The Basic Stern surface complexation model [24] and the GRFIT software [25] were used for quantitative interpretation of experimental data. The GRFIT program is very convenient because the fitting of adjustable parameters is accompanied by a graphic drawing of an adsorption curve, from which one can immediately judge how successful the choice of reaction equations and initial values of the adjustable parameters is. A first step of the work was to choose the components of the solution, solid, and charge on different planes of the interface. The components of the solution were initial species of biomolecule, proton, and electrolyte ions. The surface components are considered to be: initial amino group of chitosan ( $\equiv\text{S}-\text{NH}_2$ ) and the electrical components ( $exp0$  and  $exp1$ ), which correspond to the values of the charges of the species in the 0 and 1 planes of the interface. They were expressed as coefficients of the potentials at the respective planes of the electric double layer (EDL). The next step is a creation of a matrix in which the species present in the solution (all forms of biomolecules other than the initial one) and surface species (neutral and protonated amino groups of chitosan), ion pairs with background electrolyte ions, and surface complexes with biomolecules were defined as combinations of components. It should also be noted that the program requires knowledge of the characteristics of a solid, i.e. specific surface area and concentration of functional groups or site density. The concentration of functional groups can be set as an adjustable parameter or is selected on the basis of data.

## 2.6. Quantum-chemical calculations

In order to help explaining the mechanism of nucleotide adsorption on chitosan-silica composite the quantum-chemical calculations were employed. A model chitosan-silica substrate was chosen as a fragment of a chitosan chain containing four elementary units, one acetyl ( $\text{CH}_3\text{CO}^-$ ) group and one protonated amino ( $-\text{NH}_3^+$ ) group. The edge  $-\text{CH}_2-\text{O}-$  vacancies were terminated by methyl groups (i.e.  $-\text{CH}_2-\text{OCH}_3$ ). The whole substrate model

was considered as a positively charged (1+) cation (denoted next as  $\text{Ch}^+$ ). The nucleotide species were simulated following the structures in Table 1. Optimization of individual chitosan fragment, nucleotide species and their complexes was performed by the semi-empirical PM6 method [26] with accounting for the solvent effect (water) by means of the polarizable continuum model (PCM) [27]. For all optimized structures the vibrational frequencies were calculated. No imaginary frequencies were found in the simulated vibrational spectra meaning that the optimized structures correspond to real energy minima on potential energy surface of the singlet ground electronic state. Complexation energies ( $E_{\text{com}}$ ) were calculated by the direct method with accounting of zero-point energy ( $E_{\text{ZPE}}$ ) correction:

$$E_{\text{com}} = (E_0 + E_{\text{ZPE}})[\text{Ch}^+\text{H}_n\text{L}^{m-}] - (E_0 + E_{\text{ZPE}})[\text{Ch}^+] - (E_0 + E_{\text{ZPE}})[\text{H}_n\text{L}^{m-}]$$

where  $E_0$  denotes a total energy of the corresponding complex ( $\text{Ch}^+\text{H}_n\text{L}^{m-}$ ) and the individual  $[\text{Ch}^+]$ ,  $[\text{H}_n\text{L}^{m-}]$  counterparts. All the calculations were performed using the Gaussian 16 software [28].

### 3. Results and Discussion

#### 3.1 Synthesis and characterization of chitosan-silica material

Chitosan combined with an inorganic oxide such as silica could have the potential for concentrating molecules of different nature: extended specific surface, accessibility of functional groups and thermal stability [13,14,21]. The impregnation of fumed silica with slightly acidic chitosan solution is a rapid, effective and sustainable way of composite preparation. This approach of composites processing is in agreement with the principles of *Green Chemistry* [29,30]. The synthesized composite belongs to a hybrid material of Class I, where the organic (chitosan) and inorganic (silica) parts are combined through weak interactions, such as hydrogen bonds between the amine, acetamid or hydroxyl groups of the biopolymer and silanol groups of silica or electrostatic forces between protonated amino groups and dissociated hydroxyl groups [14,31–33].

A detailed characterization of the chitosan-silica composite was accomplished in our previous work [21]. The chitosan layer on the silica surface was confirmed by the characteristic bands in FTIR spectra of the composite (Figure S1): 1640 – 1548  $\text{cm}^{-1}$ :  $\nu(\text{C}=\text{O})$  in  $\text{NHCOCH}_3$ , Amid I; 1600 – 1400  $\text{cm}^{-1}$ :  $\delta(\text{N}-\text{H})$  in  $\text{NH}_3^+$ ; 1420  $\text{cm}^{-1}$ :  $\delta(\text{CH}_2)$  in  $\text{CH}_2\text{OH}$ ; 1380  $\text{cm}^{-1}$ :  $\delta_s(\text{CH}_3)$  in  $\text{NHCOCH}_3$ ; along with the bands related to the silica-based materials: 1097, 967  $\text{cm}^{-1}$ :  $\nu(\text{Si}-\text{O})$  of  $\text{Si}-\text{O}-\text{Si}$ , 810  $\text{cm}^{-1}$ :  $\delta(\text{Si}-\text{O})$  of  $\text{Si}-\text{O}-\text{Si}$  (Table S1). Based on the results of thermogravimetric analysis (Figure S2), the concentration of chitosan in the composite is 100  $\text{mg}\cdot\text{g}^{-1}$  (10%). This serves as an additional confirmation for a high yield (close to 100%) of the composite material. As this is well correlated with the mass ratio of pristine chitosan and fumed silica used for synthesis, it can be assumed that

the *Atom Economy* principle of Green Chemistry was successfully achieved [30]. The main thermal parameters and decomposition regions determined from TG- and DTG-curves are summarized in Table S2. According to SEM micrographs, the synthesized composite characterized by a homogeneous overlayer of the chitosan (Figure S3). The relatively high specific surface area ( $170 \text{ m}^2\cdot\text{g}^{-1}$ ) for a biopolymer-based hybrid material and its mesoporosity with an average diameter of pores around 30 nm, makes it reasonable to assume that the material can be successfully applied as a carrier for concentration of even relatively big organic molecules (Figure S4). The high potential as sorbent from aqueous solutions is also confirmed by its good stability in acidic conditions according to the conducted tests [21].

### 3.1 Chitosan surface basicity

Chitosan is a partially deacetylated derivative of chitin, a naturally occurring amino polysaccharide [34,35]. Chitosan is a linear copolymer of 2-acetoamido-2-deoxy- $\beta$ -D-glucopyranose and 2-amino-2-deoxy- $\beta$ -D-glucopyranose. Due to the presence of a primary amine on the glucosamine residues, which can be protonated in a wide range of pH, chitosan behaves in aqueous solution as a cationic polyelectrolyte. The acid-base properties of chitosan as a function of the degree of deacetylation, molecular weight, and ionic strength have been investigated by several groups [36–39]. The protonation constants ( $\log K$ ) of chitosan in aqueous solution vary from 6.3 till 7.3 depending on the degree of deacetylation, and the molecular weight of polymer. It can be assumed that chitosan attached to the surface of silica retains its ability to attach protons. According to surface complexation theory [40–42], the charging of composite surfaces as a result of its interaction with protons of an aqueous solution gives rise to an electrical double layer. This affects the complexation reactions with inorganic and organic molecules. Surface complexation models have been successfully used to describe the binding of protons and chemical species by active groups of oxide surfaces. As far as we know, the principles of the surface complexation theory have not previously been used to quantify acid-base and adsorption properties of polymers attached to the surface of a carrier. Regardless, the study of the adsorption interaction of organic or inorganic compounds dissolved in water must be preceded by a detailed investigation of the protolytic properties of the polymer surface groups [24,40–42].

We assumed that surface charge of composite under investigation is determined by the interaction of chitosan's primary amino groups with protons. We therefore treated the potentiometric titration data of composite as adsorbed proton concentrations as dependence of pH:

$$C_{ads}^H = (C_{HCl} - [H^+]) - (C_{NaOH} - [OH^-]),$$

where  $C_{HCl}$  and  $C_{NaOH}$  are the concentrations of added acid and base and  $[H^+]$  and  $[OH^-]$  are the equilibrium proton (measured as pH) and hydroxyl concentrations. These data are presented in Figure 1.

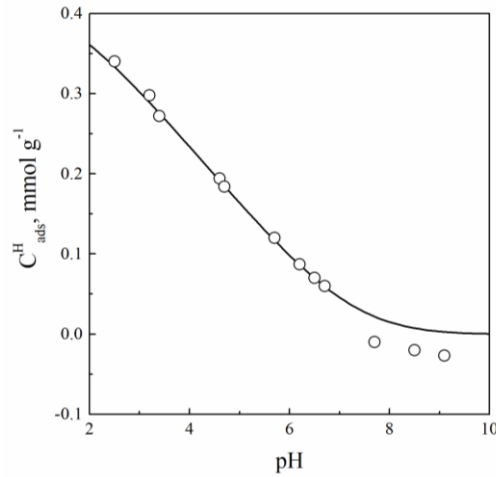
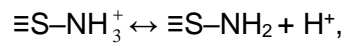


**Figure 1.** Concentrations of protons adsorbed on a chitosan-composite surface as a function of pH:  $C_{comp} = 1 \text{ g} \cdot \text{L}^{-1}$ ,  $0.01 \text{ M NaCl}$ . Symbols are experimental data, the full line is calculated curve.

These experimental data were used for surface complexation modeling to estimate the deprotonation constant of chitosan protonated amino groups according to the following reaction:



$$K_s^H = \frac{[S-\text{NH}_2][\text{H}^+]}{[S-\text{NH}_3^+]} \exp(F\Psi_0 / RT),$$

where  $[S-\text{NH}_2]$  and  $[S-\text{NH}_3^+]$  are equilibrium concentrations of neutral and protonated chitosan amino groups ( $\text{mol} \cdot \text{L}^{-1}$ ),  $\Psi_0$  is the potential of plane 0 of electric double layer,  $F$  is the Faraday constant,  $96485 \text{ C/mol}$ ;  $R$  is the universal gas constant, and  $T$  is the temperature, K.

First, we used the Diffuse Double Layer Model [24,41] and GRFIT software for fitting the surface site density and the deprotonation constant, leading to the values: surface site density is  $0.4 \text{ mmol} \cdot \text{g}^{-1}$  and  $\log K_s^H = -(6.93 \pm 0.05)$ . The concentration of active groups on the



surface, calculated on the basis of the amount of chitosan, the average molecular weight of the monomer unit, and the degree of deacetylation of 75%, is  $0.4 \text{ mmol}\cdot\text{g}^{-1}$ . The deprotonation constant of the protonated amino groups is comparable with these constants obtained for chitosan in aqueous solution [37–39].

Subsequently we used these values for fitting the capacitance of the electric double layer with the Constance Capacitance Model [24,40,42] which is related surface charge ( $\sigma_0$ ) and surface potential ( $\Psi_0$ ):

$$\sigma_0 = C_1 \Psi_0,$$

to obtain  $C_1$  equal  $0.9 \text{ F}\cdot\text{cm}^{-2}$ . All these values are required for modeling of acid-base and adsorption properties of immobilized chitosan with the Basic Stern Model (BSM) [24]. The latter makes it possible to distinguish inner- and outer sphere complexes. According to this model, the interface is divided into two regions: the compact region (extending up to several angstroms from surface) and the diffuse one, where the counter ions accumulate to compensate the surface charge (Figure 2). The compact region involves two charged planes: the surface (or plane 0) of the active surface groups and the head end of the diffuse layer of the interface (or plane 1). Potential-determining ions are adsorbed in one of them (zero plane), while weakly bound counter ions are adsorbed in another plane (plane 1). These counter-ions form electrostatic outer sphere complexes (or ions pairs) with the surface groups of opposite charge.

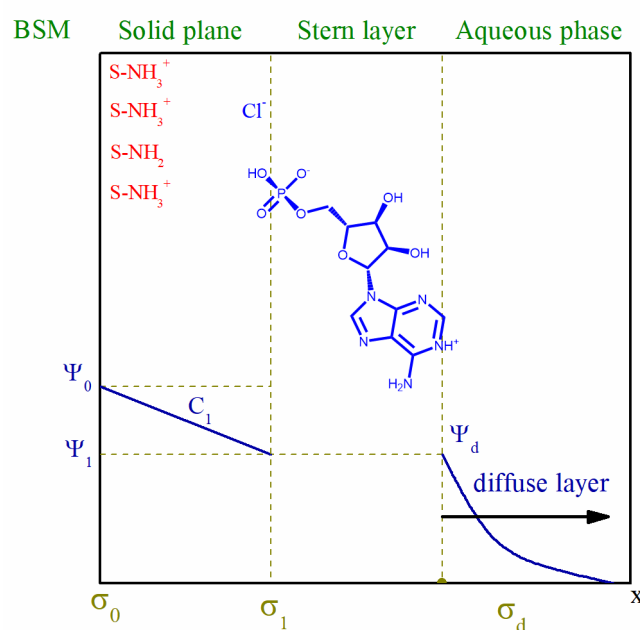
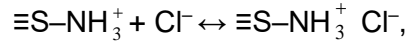


**Figure 2.** The structure of the electrical double layer (BSM) at chitosan-silica/aqueous electrolyte solution interface:  $\Psi$  is the potential;  $\sigma$  is the surface charge; charge symbols of  $\sigma_0$  and  $\sigma_1$  correspond to planes 0 and 1, respectively.

Thus, we should take into account interaction of protonated amino groups of chitosan with electrolyte anions according to the reaction:



which is characterized by the following constant:

$$K_s^{Cl} = \frac{[S - \text{NH}_3^+ \text{Cl}^-]}{[S - \text{NH}_3^+][\text{Cl}^-]} \exp(F(\Psi_0 - \Psi_1)/RT),$$

where  $\Psi_0$  and  $\Psi_1$  are the potentials in plane 0 and 1 respectively. The fitting of experimental potentiometric data with all obtained values of surface site density, deprotonation constant, and capacitance of EDL gives the ion pair formation constant,  $\log K_s^{Cl} = (1.35 \pm 0.05)$ . In Figure 1 the calculated curve is shown as a line. It should be noted that this calculated line is in good agreement with experimental data. In the region of  $\text{pH} > 7$ , small negative charge values are observed. Most likely, ionization of silanol groups of silica used as a substrate is manifested in this region. It is difficult to quantify the contribution of the ionization of silanol groups, since their exact concentration is unknown. In further calculations, studying the nucleotide adsorption, we have neglected the possible ionization of the silanol groups.

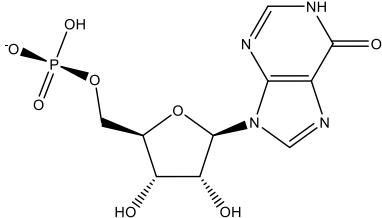
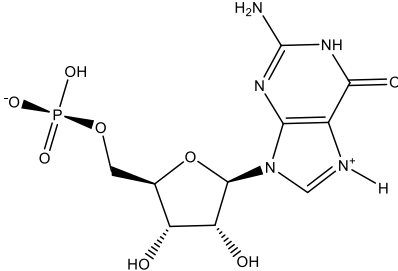
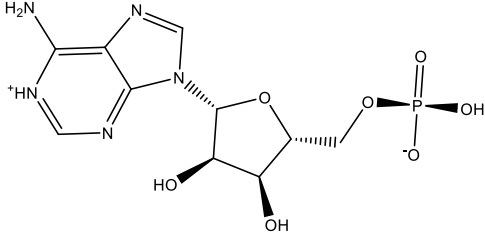
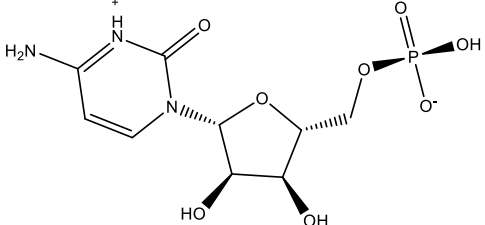
### 3.2. Nucleotide adsorption

The interaction of nucleotides with the surface of the chitosan-silica composite in aqueous electrolyte solution was interpreted as the formation of adsorption complexes. To select possible complexation reactions it is necessary to take into account not only the state of the functional groups of the solid, but also the forms in which the solutes being adsorbed are present in solution depending on pH. Nucleotides consist of a heterocyclic base (purine or pyrimidine), in which a hydrogen atom at one of nitrogen atom (N-1 for pyrimidine, or N-9 for purine bases) is replaced by a phosphorylated carbohydrate residue. Apart from the common bases adenine and guanine (purine), and cytosine and uracil (pyrimidine), nucleic acids may contain “minor” base hypoxanthine (corresponding nucleotide is inosine phosphate) and orotic acid (nucleotide is orotidine phosphate). All these nucleotides were tested at the adsorption study from aqueous solution.

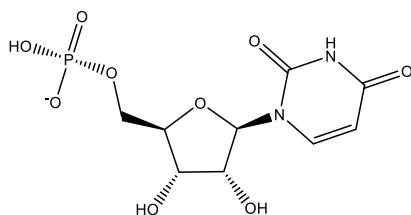
The structures of the studied nucleotides as monophosphates and their ionization constants are presented in Table 1. Considering the acid-base properties of the nucleotides in more

detail, we note that the phosphate groups in the nucleoside monophosphates are characterized by two ionization constants: primary group dissociates at  $\text{pH} < 2$ , while the secondary one is ionized at  $\text{pH} > 6$  [43,44]. In the studied purine and pyrimidine nucleotides, nitrogen atoms of the heterocyclic ring differ significantly in their basicity. Proton releases from the  $\text{N}_1\text{-H}^+$  group of adenosine-5'-monophosphate, and from  $\text{N}_3\text{-H}^+$  of cytidine-5'-monophosphate occur at  $\text{pH} \sim 4$ . The deprotonation of the  $\text{N}_7\text{-H}^+$  group of guanosine-5'-monophosphate is observed at  $\text{pH} > 2.3$ , while the  $\text{N}_7$  nitrogen atom of inosine-5'-monophosphate is protonated in highly acidic solution. The pyrimidine heterocycle of orotidine-5'-monophosphate contains an additional carboxyl group which is ionized at  $\text{pH} > 2.4$ .

**Table 1.** Ionization constants of nucleotides

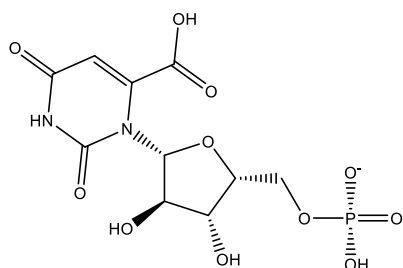
Nucleotide	Ionization constant, $\text{p}K(0.01 \text{ M})$
 inosine-5'-monophosphate, $\text{HL}^-$ (IMP)	6.47 ( $-\text{PO}_3\text{H}^-$ )
 guanosine-5'- monophosphate, $\text{H}_2\text{L}^+$ (GMP)	2.48 ( $-\text{N}_7\text{H}^+$ ) 6.48 ( $-\text{PO}_3\text{H}^-$ )
 adenosine-5'- monophosphate, $\text{H}_2\text{L}^+$ (AMP)	3.96 ( $-\text{N}_1\text{H}^+$ ) 6.46 ( $-\text{PO}_3\text{H}^-$ )
	4.31 ( $-\text{N}_3\text{-H}^+$ ) 6.15 ( $-\text{PO}_3\text{H}^-$ )

cytidine-5'- monophosphate,  $\text{H}_2\text{L}^\pm$  (CMP)



6.04 ( $-\text{PO}_3\text{H}^-$ )

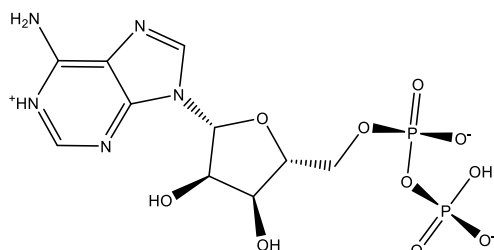
uridine-5'- monophosphate,  $\text{HL}^-$  (UMP)



2.4 ( $-\text{COOH}$ )

6.10 ( $-\text{PO}_3\text{H}^-$ )

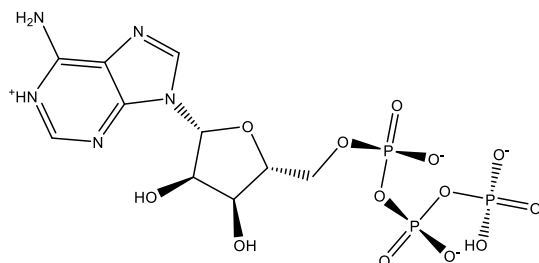
orotidine-5'- monophosphate,  $\text{H}_2\text{L}^-$  (OMP)



4.21 ( $-\text{N}_1\text{H}^+$ )

6.71 ( $-\text{P}_2\text{O}_6\text{H}^-$ )

adenosine-5'- diphosphate,  $\text{H}_2\text{L}^\pm$  (ADP)



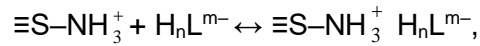
4.38 ( $-\text{N}_1\text{H}^+$ )

6.96 ( $-\text{P}_3\text{O}_9\text{H}^-$ )

adenosine-5'- triphosphate,  $\text{H}_2\text{L}^\pm$  (ATP)

All these acid-base properties of the nucleotides under investigation are reflected in the solution speciation diagrams presented in Figure 3. The solution speciations show in which forms, depending on pH, the studied nucleotides are present in solution. At pH 2 initial forms of AMP and CMP are zwitterionic ( $\text{NH}^+$ ,  $\text{PO}_3\text{H}^-$ ). The fraction of zwitterions for GMP is smaller due to lower value of the deprotonation constant of the  $\text{N}_7\text{--H}^+$  group in comparison with these values for AMP and CMP. The initial forms of IMP and UMP are monoanions. In acid solution the OMP exists as dianion due to ionization of the additional carboxyl group ( $\text{COO}^-$ ,  $\text{PO}_3\text{H}^-$ ). The initial forms of the adenosine-5'-di- and triphosphates are doubly and triply charged anions, respectively. With increasing pH further ionization of the initial forms is observed with the formation of the corresponding anions with higher charges.

Adsorption of all nucleotides from 0.01 M NaCl solution was studied as a function of pH (Figure 3). The adsorption of all nucleotides decreases with increasing pH. The adsorption curves of AMP, GMP, and CMP pass through a maximum whose position on the pH scale corresponds to the ionization constant of the zwitterion. The presence of anionic forms of nucleotides in solutions suggests that the main contribution to the adsorption on the composite surface comes from the electrostatic interaction with positively charged amino groups of chitosan according to:



$$K = \frac{[S - \text{NH}_3^+ \text{H}_n\text{L}^{m-}]}{[S - \text{NH}_3^+][\text{H}_n\text{L}^{m-}]} \exp(F(\Psi_o - m\Psi_1)/RT)$$

where  $\text{H}_n\text{L}^{m-}$  is initial form of nucleotide, n and m are dependent on nature of nucleotides (for details see Table 2).

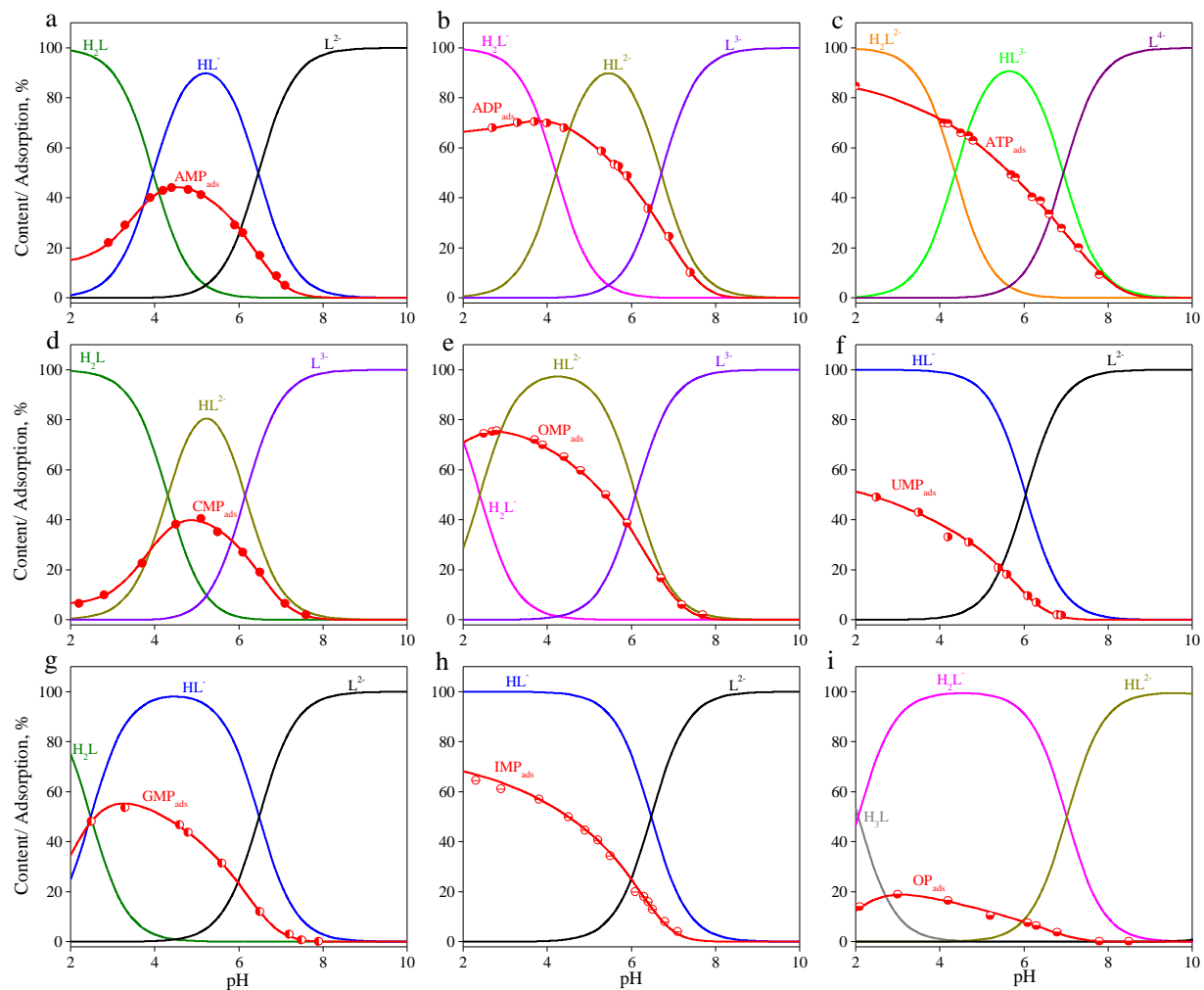


**Figure 3.** Solution speciations and adsorption curves of nucleotides: (a) AMP, (b) ADP, (c) ATP, (d) CMP, (e) OMP, (f) UMP, (g) GMP, (h) IMP and (i) OP.  $C_{\text{sorbate}} = 0.1 \text{ mmol}\cdot\text{L}^{-1}$ ,  $C_{\text{composite}} = 1 \text{ g}\cdot\text{L}^{-1}$ . Symbols are experimental adsorption data, lines are calculated adsorption curves.

**Table 2.** Experimentally measured surface complex formation constants of nucleotides and orthophosphate (in logK units) vs. theoretically calculated complexation energies ( $E_{\text{com}}$ ).

Nucleotide	Surface reactions	$\log K \pm 0.05$	$E_{\text{com}},$ $\text{kcal} \cdot \text{mol}^{-1}$
AMP	$\equiv\text{S}-\text{NH}_3^+ + \text{H}_2\text{L}^\pm \leftrightarrow \equiv\text{S}-\text{NH}_3^+ \text{H}_2\text{L}^\pm$	3.18	15.3
	$\equiv\text{S}-\text{NH}_3^+ + \text{HL}^- \leftrightarrow \equiv\text{S}-\text{NH}_3^+ \text{HL}^-$	3.31	15.4
CMP	$\equiv\text{S}-\text{NH}_3^+ + \text{H}_2\text{L}^\pm \leftrightarrow \equiv\text{S}-\text{NH}_3^+ \text{H}_2\text{L}^\pm$	2.96	14.1
	$\equiv\text{S}-\text{NH}_3^+ + \text{HL}^- \leftrightarrow \equiv\text{S}-\text{NH}_3^+ \text{HL}^-$	3.28	14.0
GMP	$\equiv\text{S}-\text{NH}_3^+ + \text{HL}^- \leftrightarrow \equiv\text{S}-\text{NH}_3^+ \text{HL}^-$	3.22	16.1
IMP	$\equiv\text{S}-\text{NH}_3^+ + \text{HL}^- \leftrightarrow \equiv\text{S}-\text{NH}_3^+ \text{HL}^-$	3.27	16.6
UMP	$\equiv\text{S}-\text{NH}_3^+ + \text{HL}^- \leftrightarrow \equiv\text{S}-\text{NH}_3^+ \text{HL}^-$	2.69	11.5
OMP	$\equiv\text{S}-\text{NH}_3^+ + \text{HL}^{2-} \leftrightarrow \equiv\text{S}-\text{NH}_3^+ \text{HL}^{2-}$	3.03	16.6
ADP	$\equiv\text{S}-\text{NH}_3^+ + \text{H}_2\text{L}^- \leftrightarrow \equiv\text{S}-\text{NH}_3^+ \text{H}_2\text{L}^-$	3.11	16.1
	$\equiv\text{S}-\text{NH}_3^+ + \text{HL}^{2-} \leftrightarrow \equiv\text{S}-\text{NH}_3^+ \text{HL}^{2-}$	3.52	20.8
ATP	$\equiv\text{S}-\text{NH}_3^+ + \text{H}_2\text{L}^{2-} \leftrightarrow \equiv\text{S}-\text{NH}_3^+ \text{H}_2\text{L}^{2-}$	3.38	22.9
	$\equiv\text{S}-\text{NH}_3^+ + \text{HL}^{3-} \leftrightarrow \equiv\text{S}-\text{NH}_3^+ \text{HL}^{3-}$	4.02	23.0
OP	$\equiv\text{S}-\text{NH}_3^+ + \text{H}_2\text{L}^- \leftrightarrow \equiv\text{S}-\text{NH}_3^+ \text{H}_2\text{L}^-$	2.39	12.0

The modeling of the acid-base properties of solid and adsorption curves with the GRFIT program begins with a matrix of components. This interaction leads to the formation of all species in the systems. The active surface sites of the solid, protons, an adsorbate and background electrolyte ions are among the material components. The matrix of components is supplemented with *exp0* and *exp1* electric components corresponding to the particle charge in plane 0 and 1, respectively. It is important to choose an appropriate initial form of the adsorbate because any form of nucleotide present in solution can be chosen as the initial one. The surface complexation reactions and their equilibrium constants may be written in different manner depending on the choice of an initial particle. The best agreement between experimental data and calculated adsorption curves was achieved for complex formation

reactions presented in Table 2. These calculated adsorption curves for all nucleotides are shown in Figure 3 as solid lines connected experimental points.

The nucleotide anions and zwitterions (of AMP and CMP only) form outer-sphere electrostatic complexes with protonated amino groups of chitosan. The values of the complex formation constants of the singly charged anion of all nucleotides are almost the same regardless of the nucleotide nature. This can be explained by the fact that a phosphate group of the nucleotides takes part in the electrostatic interaction. The protolytic properties are practically the same for all nucleotides. The higher the charge of an anion forming a complex with a protonated group, the higher the stability constant of the complex, a regularity that is typical for electrostatic interactions. Therefore, ATP complexes are stronger than AMP complexes. The same observation was made in the study by Stefano et al. [45] devoted to the interaction of ATP and AMP with chitosan in an aqueous solution.

The orthophosphate (OP) adsorption on the surface of the chitosan-silica composite was studied for comparison with the nucleotides. As can be seen from Table 2, the complex formation constant of the orthophosphate monoanion is much smaller than the nucleotide constants. This indicates that not only the phosphate group determines the strength of the nucleotide binding to the surface, it also seems that the heterocyclic base and saccharide can form other types of bonds.

Indeed, as follows from our quantum-chemical PM6 calculations the saccharide fragment form quite short H-bonds with the chitosan substrate ( $\text{Ch}^+$ , Figure 4), while the heterocyclic bases are quite far from the chitosan surface and does actually not interact with it. We also observe a clear correlation between the experimentally estimated complex formation constant and calculated complexation energies (Table 2). We find that the OP and UMP species demonstrate the smallest complex formation constants ( $\log K=2.39$  and  $2.69$ , respectively) and smallest calculated complexation energies ( $E_{\text{com}}=12.0$  and  $11.5 \text{ kcal}\cdot\text{mol}^{-1}$ ). Multicharged nucleotides, like ADP in  $\text{HL}^{2-}$  form, ATP in  $\text{HL}^{3-}$  form and ATP in  $\text{HL}^{2-}$  form generally demonstrate higher complex formation constants ( $\log K=3.52$ ,  $3.38$  and  $4.03$ ) than the zwitterionic and anionic nucleotides ( $\log K$  varies within the short range  $2.69\text{--}3.31$ ). Such a trend is also reproduced in our PM6 calculations – complexation energies are highest for ADP in  $\text{HL}^{2-}$  form ( $-20.8 \text{ kcal}\cdot\text{mol}^{-1}$ ), ATP in  $\text{HL}^{3-}$  form ( $-23.0 \text{ kcal}\cdot\text{mol}^{-1}$ ) and ATP in  $\text{HL}^{2-}$  form ( $-22.9 \text{ kcal}\cdot\text{mol}^{-1}$ ). This is due to the stronger electrostatic interaction between the positive charge localized on  $-\text{NH}_3^+$  group of the  $\text{Ch}^+$  substrate model and multiple negative charges localized on the phosphate groups of the studied nucleotides (Figure 4). An exception is OMP dianion where the complex formation constant is quite small ( $\log K=3.03$ ) as well as the calculated  $E_{\text{com}}$  value being in a moderate region ( $16.6 \text{ kcal}\cdot\text{mol}^{-1}$ ). This is because of OMP possesses a two-center dianionic structure in which one negative charge is localized on the  $\text{PO}_3\text{H}^-$  group, while the second one is localized on the  $\text{COO}^-$  moiety. The



latter does not directly interact with the chitosan substrate (Figure 4). For the remaining monoanionic and zwitterionic nucleotides, a calculated complexation energy varied only within the range (11.5–16.6 kcal·mol<sup>-1</sup>) in agreement with experimental observations (logK=2.69–3.31).

The analysis of the structures for all optimized complexes reveals that for all monophosphates (OMP, UMP, CMP, AMP, GMP, IMP) and for the only one diphosphate (ADP in monoanionic form), the saccharide fragment plays an important role in the binding of the nucleotides to the chitosan surface. For the dianionic ADP and both studied triphosphates (ATP in HL<sup>3-</sup> and HL<sup>2-</sup>-forms) the saccharide unit is far from the chitosan substrate and does not directly interact with it (Figure 4). This fact additionally confirms the key role of the electrostatic interactions between the surface-located NH<sub>3</sub><sup>+</sup> groups and –PO<sub>3</sub>H<sup>-</sup>/–PO<sub>3</sub><sup>2-</sup> fragments of the nucleotides in the adsorption mechanism of ADP (HL<sup>2-</sup>) and ATP (HL<sup>2-</sup>, HL<sup>3-</sup>) nucleotides.

The adsorption of most of the studied nucleotides is determined by the formation of one surface complex. Figure 5 shows distribution diagrams of the surface complexes of those nucleotides forming two surface species. The concentrations of complexes containing zwitterionic forms of AMP and CMP are significantly lower than those of the anionic complexes. The content of the complexes of the various anions of ADP and ATP in the surface layer is determined by their distribution in the aqueous solution.

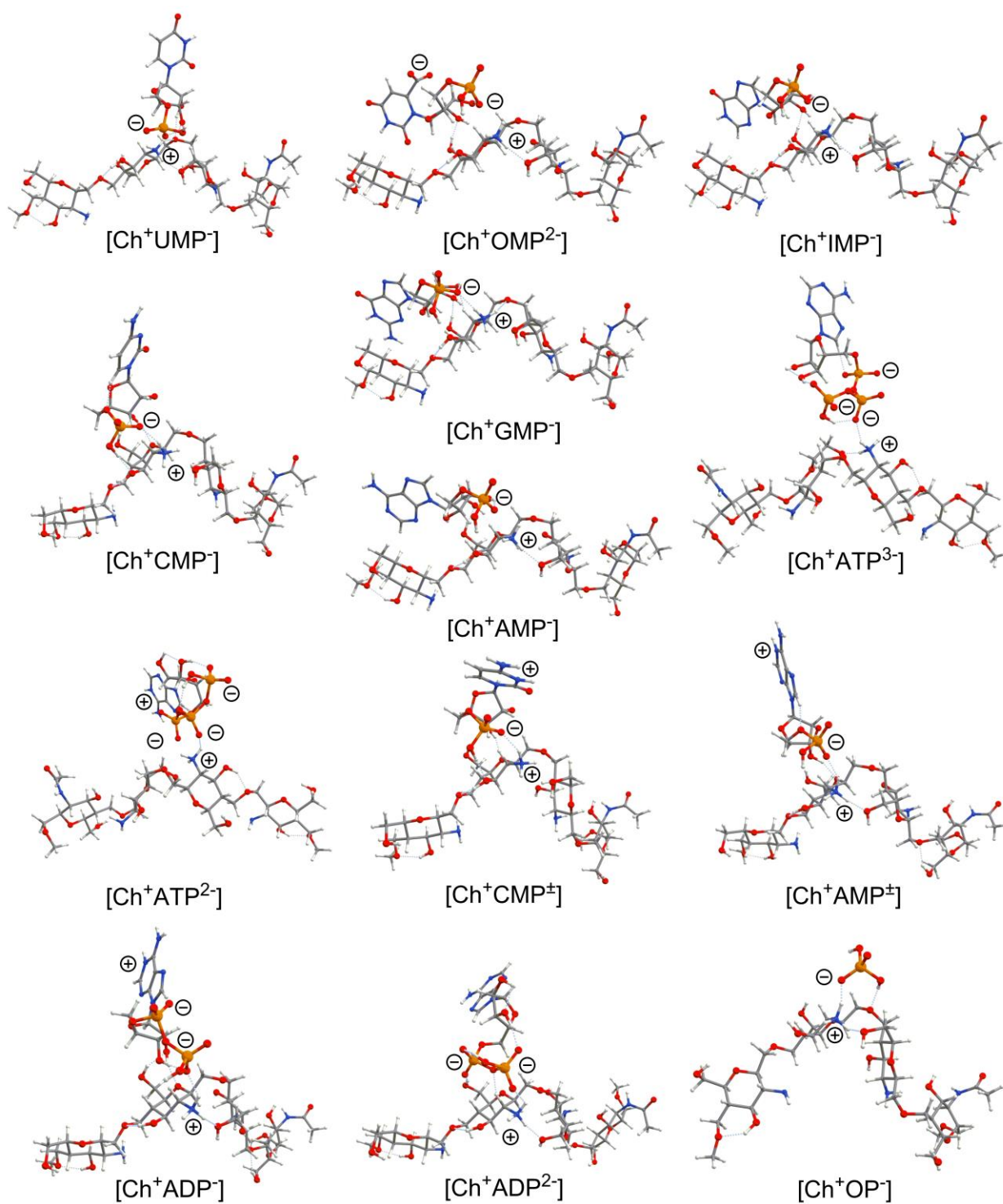


**Figure 4.** PM6 method optimized structures of chitosan-nucleotide complexes. Predominant localizations of positive and negative charges are also marked for each complex.

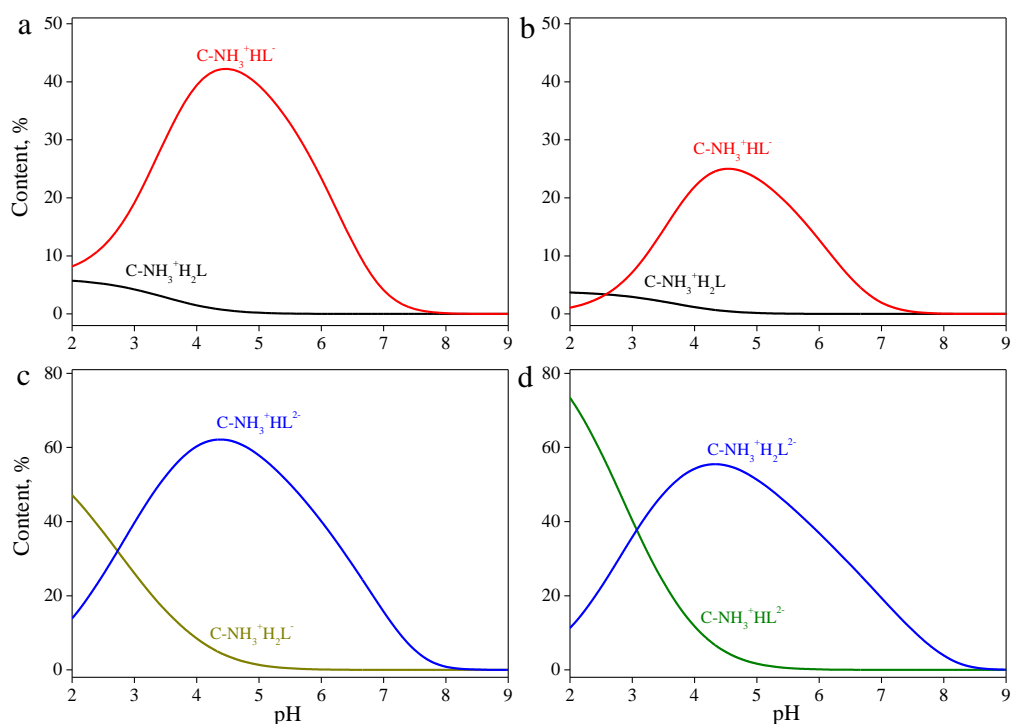


**Figure 5.** Distribution diagrams of complexes of (a) AMP, (b) CMP, (c) ADP, and (d) ATP formed on the surface of chitosan-containing silica.

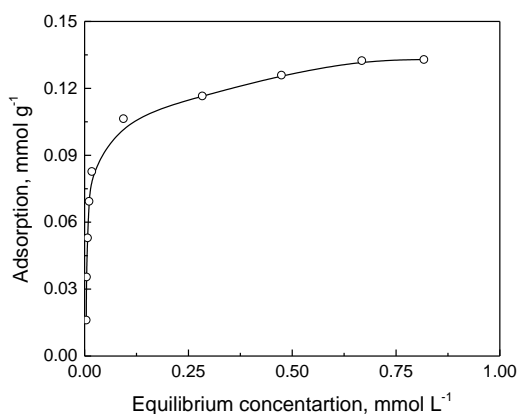


**Figure 6.** Isotherm of adsorption of ATP by chitosan-silica composite (concentration of composite  $1 \text{ g} \cdot \text{L}^{-1}$ , pH 3.5).

The effect of initial ATP nucleotide concentration on the adsorption capacity of the composite surface was studied in acidic media (pH 3.5) in the range of initial nucleotide concentration from 0.2 to  $1 \text{ mmol} \cdot \text{L}^{-1}$ . The surface of the synthesized chitosan-silica composite has high affinity to the ATP nucleotide molecule (Figure 6). The distribution

coefficient was found to be  $4.08 \text{ L}\cdot\text{g}^{-1}$ , which is higher than for organic molecules adsorbed by variable adsorbents reported in literature. The shape of the isotherm confirms an L-type of isotherm produced by monolayer adsorption on a homogeneous surface with no interaction between the adsorbed molecules. This observation is also confirmed by the good correlation of experimental data with the Langmuir isotherm model due to high values of the regression coefficient ( $R^2=0.9985$ ). Calculated parameters from the Langmuir, Freundlich and Temkin isotherm models for adsorption of ATP nucleotides on a synthesized chitosan-silica composite are summarized in Table 3. Based on the obtained values of the correlation coefficient, all applied isotherm models are consistent with the experimental data for the chosen range of initial nucleotide concentrations. The monolayer capacity was found to be  $0.13 \text{ mmol}\cdot\text{g}^{-1}$  for the ATP nucleotide. The adsorption was found to be favorable according to positive value of  $R_L$  ( $0 < R_L < 1$ ). The heat of adsorption ( $b_T$ ) of ATP on the composite was found to be higher ( $822.8 \text{ J}\cdot\text{mol}^{-1}$ ) than for other complex organic molecules, for example, bile acids [21]. The low value of the maximum binding energy for the interactions between the composite surface and the ATP molecule ( $K_T=1.906 \text{ L}\cdot\text{g}^{-1}$ ) is in line with the assumption of high affinity of the studied nucleotide to the chitosan deposited on the silica surface.

**Table 3.** Langmuir, Freundlich and Temkin isotherm model parameters for adsorption of ATP by chitosan-silica composite (concentration of composite  $1 \text{ g}\cdot\text{L}^{-1}$ , pH 3.5).

Isotherm model	Parameter	Values
Langmuir	$q_0, \text{ mmol}\cdot\text{g}^{-1}$	0.13
	$K_L, \text{ L}\cdot\text{mg}^{-1}$	51.1
	$R_L,$	$0.98\cdot 10^{-4}$
	$R^2$	0.9985
Freundlich	$K_F, \text{ mmol}\cdot\text{g}^{-1}$	6.05
	$n$	3.654
	$1/n$	0.274
	$R^2$	0.7418
Temkin	$b_T, \text{ J}\cdot\text{mol}^{-1}$	822.8
	$K_T, \text{ L}\cdot\text{g}^{-1}$	1.906
	$R^2$	0.9528

## Conclusion.

A composite based on chitosan and silica was found to be a prospective carrier for mono-, di- and triphosphate nucleotides. It was shown from the adsorption study that the nucleotides have high affinity to the chitosan-silica surface, which was confirmed by the high distribution coefficient:  $4.08 \text{ L}\cdot\text{g}^{-1}$ . Based on applied isotherm models, the monolayer adsorption occurred in under relatively low value of the maximum binding energy for interactions between the composite surface and nucleotide molecule:  $1.906 \text{ L}\cdot\text{g}^{-1}$  for ATP nucleotide. The measured surface complex formation constants of the nucleotides were found to be higher than for the orthophosphate. These experimental observations were confirmed by high values of theoretically computed nucleotide complexation energies for chitosan deposited on the surface comparing to the system chitosan:orthophosphate. It was determined from quantum-chemical PM6 calculations that the electrostatic interactions between the surface-located protonated amino groups and the negatively charged P-containing fragments of the nucleotides play a decisive role in their adsorption. In case of nucleotides in the monoanionic form, the saccharide fragment could take part in the adsorption through creation of hydrogen bonds. These results demonstrate that chitosan-silica composites are highly promising materials as bio-carriers in gene therapy.

## Acknowledgements

A.S. thanks for financial support from MISTRA (project: SafeChem). HÅ and GB thanks for support to Olle Engkvist Byggmästare foundation (contract no. 189-0223). GB also thanks for the support to the Ministry of Education and Science of Ukraine (projects no. 0117U003908). The quantum-chemical calculations were performed with computational resources provided by the High Performance Computing Center North (HPC2N) in Umeå, Sweden, through the project "Multiphysics Modeling of Molecular Materials" SNIC 2019/2-41.

## Competing Interests

The authors declare that they have no known competing financial interests or personal relationships which have, or could be perceived to have, influenced the work reported in this article.

## References

- [1] Y. Cao, Y.F. Tan, Y.S. Wong, M.W.J. Liew, S. Venkatraman, Recent Advances in Chitosan-Based Carriers for Gene Delivery, *Mar. Drugs*. 17 (2019) 381. <https://doi.org/10.3390/md17060381>.
- [2] A.J. Varma, S. V Deshpande, J.F. Kennedy, Metal complexation by chitosan and its

- derivatives: a review, *Carbohydr. Polym.* 55 (2004) 77–93.
- [3] M.N.V.R. Kumar, A review of chitin and chitosan applications, *React. Funct. Polym.* 46 (2000) 1–27.
  - [4] S. Babel, T.A. Kurniawan, Low-cost adsorbents for heavy metals uptake from contaminated water: a review, *J. Hazard. Mater.* 97 (2003) 219–243.
  - [5] G. Crini, Recent developments in polysaccharide-based materials used as adsorbents in wastewater treatment, *Prog. Polym. Sci.* 30 (2005) 38–70.
  - [6] V. Dodane, V.D. Vilivalam, Pharmaceutical applications of chitosan, *Pharm. Sci. Technol. Today.* 1 (1998) 246–253.
  - [7] M. Ramamoorth, A. Narvekar, Non viral vectors in gene therapy-an overview, *J. Clin. Diagnostic Res. JCDR.* 9 (2015) GE01.
  - [8] J.-W. Shen, J. Li, Z. Zhao, L. Zhang, G. Peng, L. Liang, Molecular dynamics study on the mechanism of polynucleotide encapsulation by chitosan, *Sci. Rep.* 7 (2017) 1–9.
  - [9] S. Mao, W. Sun, T. Kissel, Chitosan-based formulations for delivery of DNA and siRNA, *Adv. Drug Deliv. Rev.* 62 (2010) 12–27.
  - [10] M.-K. Lee, S.-K. Chun, W.-J. Choi, J.-K. Kim, S.-H. Choi, A. Kim, K. Oungbho, J.-S. Park, W.S. Ahn, C.-K. Kim, The use of chitosan as a condensing agent to enhance emulsion-mediated gene transfer, *Biomaterials.* 26 (2005) 2147–2156.
  - [11] X.Z. Shu, K.J. Zhu, The influence of multivalent phosphate structure on the properties of ionically cross-linked chitosan films for controlled drug release, *Eur. J. Pharm. Biopharm.* 54 (2002) 235–243.
  - [12] Y. Gao, Z. Xu, S. Chen, W. Gu, L. Chen, Y. Li, Arginine-chitosan/DNA self-assemble nanoparticles for gene delivery: In vitro characteristics and transfection efficiency, *Int. J. Pharm.* 359 (2008) 241–246.
  - [13] M. Blachnio, T.M. Budnyak, A. Derylo-Marczewska, A.W. Marczewski, V.A. Tertykh, Chitosan-Silica Hybrid Composites for Removal of Sulfonated Azo Dyes from Aqueous Solutions, *Langmuir.* 34 (2018) 2258–2273.  
<https://doi.org/10.1021/acs.langmuir.7b04076>.
  - [14] T.M. Budnyak, M. Blachnio, A. Slabon, A. Jaworski, V.A. Tertykh, A. Derylo-Marczewska, A.W. Marczewski, Chitosan Deposited onto Fumed Silica Surface as Sustainable Hybrid Biosorbent for Acid Orange 8 Dye Capturing: Effect of Temperature in Adsorption Equilibrium and Kinetics, *J. Phys. Chem. C.* 124 (2020) 15312–15323.
  - [15] M. Vakili, M. Rafatullah, B. Salamatinia, A. Zuhairi, M. Hakimi, K. Bing, Z. Gholami, P. Amouzgar, Application of chitosan and its derivatives as adsorbents for dye removal from water and wastewater : A review, *Carbohydr. Polym.* 113 (2014) 115–130.  
<https://doi.org/10.1016/j.carbpol.2014.07.007>.

- [16] A.J. Varma, S. V Deshpande, J.F. Kennedy, Metal complexation by chitosan and its derivatives : a review, 55 (2004) 77–93. <https://doi.org/10.1016/j.carbpol.2003.08.005>.
- [17] W.S. Wan Ngah, L.C. Teong, M. a K.M. Hanafiah, Adsorption of dyes and heavy metal ions by chitosan composites: A review, Carbohydr. Polym. 83 (2011) 1446–1456. <https://doi.org/10.1016/j.carbpol.2010.11.004>.
- [18] N.M. Julkapli, H. Akil, Z. Ahmad, Preparation , Properties and Applications of Chitosan-Based Biocomposites / Blend Materials : A Review, (2012) 37–41.
- [19] I.M. El-sherbiny, N.M. El-baz, A Review on Bionanocomposites Based on Chitosan and Its Derivatives for Biomedical Applications, 2015. <https://doi.org/10.1007/978-81-322-2473-0>.
- [20] G.Z. Kyzas, D.N. Bikiaris, Recent Modifications of Chitosan for Adsorption Applications :, (2015) 312–337. <https://doi.org/10.3390/md13010312>.
- [21] T.M. Budnyak, N.N. Vlasova, L.P. Golovkova, A. Slabon, V.A. Tertykh, Bile acids adsorption by chitoan-fumed silica enterosorbent, Colloid Interface Sci. Commun. 32 (2019) 100194. <https://doi.org/https://doi.org/10.1016/j.colcom.2019.100194>.
- [22] I. Langmuir, The Constitution and Fundamental Properties of Solids and Liquids. Part I. Solids, J. Am. Chem. Soc. 38 (1916) 2221–2295.
- [23] H. Freundlich, Über die Adsorption in Lösungen, Zeitschrift Für Phys. Chemie. 57U (2017). <https://doi.org/10.1515/zpch-1907-5723>.
- [24] J. Westall, H. Hohl, A comparison of electrostatic models for the oxide/solution interface, Adv. Colloid Interface Sci. 12 (1980) 265–294.
- [25] C. Ludwig, GRFIT, a program for solving speciation problems: evaluation of equilibrium constants, concentrations and other physical parameters, 1992.
- [26] J.J.P. Stewart, Optimization of parameters for semiempirical methods V: Modification of NDDO approximations and application to 70 elements, J. Mol. Model. 13 (2007) 1173–1213. <https://doi.org/10.1007/s00894-007-0233-4>.
- [27] S. Miertuš, E. Scrocco, J. Tomasi, Electrostatic interaction of a solute with a continuum. A direct utilizaion of AB initio molecular potentials for the prevision of solvent effects, Chem. Phys. 55 (1981) 117–129. [https://doi.org/https://doi.org/10.1016/0301-0104\(81\)85090-2](https://doi.org/https://doi.org/10.1016/0301-0104(81)85090-2).
- [28] M.J. Frisch, G.W. Trucks, H.B. Schlegel, G.E. Scuseria, M. a. Robb, J.R. Cheeseman, G. Scalmani, V. Barone, G. a. Petersson, H. Nakatsuji, X. Li, M. Caricato, a. V. Marenich, J. Bloino, B.G. Janesko, R. Gomperts, B. Mennucci, H.P. Hratchian, J. V. Ortiz, a. F. Izmaylov, J.L. Sonnenberg, Williams, F. Ding, F. Lipparini, F. Egidi, J. Goings, B. Peng, A. Petrone, T. Henderson, D. Ranasinghe, V.G. Zakrzewski, J. Gao, N. Rega, G. Zheng, W. Liang, M. Hada, M. Ehara, K. Toyota, R. Fukuda, J. Hasegawa, M. Ishida, T. Nakajima, Y. Honda, O. Kitao, H. Nakai, T. Vreven, K.

- Throssell, J. a. Montgomery Jr., J.E. Peralta, F. Ogliaro, M.J. Bearpark, J.J. Heyd, E.N. Brothers, K.N. Kudin, V.N. Staroverov, T. a. Keith, R. Kobayashi, J. Normand, K. Raghavachari, a. P. Rendell, J.C. Burant, S.S. Iyengar, J. Tomasi, M. Cossi, J.M. Millam, M. Klene, C. Adamo, R. Cammi, J.W. Ochterski, R.L. Martin, K. Morokuma, O. Farkas, J.B. Foresman, D.J. Fox, G16\_A03, (2016) Gaussian 16, Revision A.03, Gaussian, Inc., Wallingford CT.
- [29] P.T. Anastas, J.B. Zimmerman, Peer reviewed: design through the 12 principles of green engineering, (2003).
- [30] P.T. Anastas, J.C. Warner, Principles of green chemistry, Green Chem. Theory Pract. (1998) 29–56.
- [31] V. Puchol, J. El Haskouri, J. Latorre, C. Guillem, A. Beltran, D. Beltran, P. Amoros, Biomimetic chitosan-mediated synthesis in heterogeneous phase of bulk and mesoporous silica nanoparticles, Chem. Commun. (2009) 2694–2696.
- [32] H. Zou, S. Wu, J. Shen, Polymer/silica nanocomposites: preparation, characterization, properties, and applications, Chem. Rev. 108 (2008) 3893–3957.
- [33] P. Chassary, T. Vincent, E. Guibal, Metal anion sorption on chitosan and derivative materials: a strategy for polymer modification and optimum use, React. Funct. Polym. 60 (2004) 137–149.
- [34] G.A.F. Roberts, Chitin chemistry, Macmillan International Higher Education, 1992.
- [35] R.A.A. Muzzarelli, M.G. Peter, Chitin handbook, Atec, 1997.
- [36] P. Sorlier, A. Denuzière, C. Viton, A. Domard, Relation between the degree of acetylation and the electrostatic properties of chitin and chitosan, Biomacromolecules. 2 (2001) 765–772.
- [37] D. Filion, M. Lavertu, M.D. Buschmann, Ionization and solubility of chitosan solutions related to thermosensitive chitosan/glycerol-phosphate systems, Biomacromolecules. 8 (2007) 3224–3234.
- [38] S. Cataldo, F. Crea, A. Gianguzza, A. Pettignano, D. Piazzese, Solubility and acid-base properties and activity coefficients of chitosan in different ionic media and at different ionic strengths, at T= 25 C, J. Mol. Liq. 148 (2009) 120–126.
- [39] Q.Z. Wang, X.G. Chen, N. Liu, S.X. Wang, C.S. Liu, X.H. Meng, C.G. Liu, Protonation constants of chitosan with different molecular weight and degree of deacetylation, Carbohydr. Polym. 65 (2006) 194–201.
- [40] W. Stumm, Aquatic surface chemistry: Chemical processes at the particle-water interface, John Wiley & Sons, 1987.
- [41] D.A. Dzombak, F.M.M. Morel, Surface complexation modeling: hydrous ferric oxide, John Wiley & Sons, 1990.
- [42] J.A. Davis, Surface complexation modeling in aqueous geochemistry, Review in



- Mineralogy. 23 (1990) 177–259.
- [43] R.M. Smith, A.E. Martell, Y. Chen, Critical evaluation of stability constants for nucleotide complexes with protons and metal ions and the accompanying enthalpy changes, *Pure Appl. Chem.* 63 (1991) 1015–1080.
- [44] W. Saenger, *Principles of nucleic acid structure*, Springer Science & Business Media, 2013.
- [45] C. De Stefano, A. Gianguzza, D. Piazzese, S. Sammartano, Speciation of chitosan–phosphate and chitosan–nucleotide systems in NaCl aqueous solution, *Chem. Speciat. Bioavailab.* 22 (2010) 99–107.